Electronic Supplementary Information (ESI)

Highly Active Conversion of CO_2 to CO on AuCuB materials

Yuting Liu‡ [a], Yuan Fang‡ [a], Qinghong Yuan* [b], Jiaxing Lu [a,c] and Huan Wang* [a,c]

a. Shanghai Key Laboratory of Green Chemistry and Chemical Process, School of Chemistry and Molecular Engineering, East China Normal University, 3663 North Zhongshan Rd., Shanghai 200062, China. E-mail: hwang@chem.ecnu.edu.cn

b. State Key Laboratory of Precision Spectroscopy, School of Physics and Electronic Science, East China Normal University, 500 Dongchuan Road, Shanghai 200241, China. E-mail: qhyuan@phy.ecnu.edu.cn

c. Institute of Eco-Chongming 20 Cuiniao Road, Chenjia Town, Chongming District, Shanghai 202162, China

Table of Contents

Experimental Procedures

Chemicals and Reagents

Sodium borohydride ($NaBH_4$, 98%), copper chloride dehydrate ($CuCl_2 \cdot 2H_2O$, >99%), potassium hydroxide (KOH, 95%) were purchased from Sinopharm. Hydrogen tetrachloroaurate (III) trihydrate ($HAuCl_4 \cdot H_2O$) was obtained from Aladdin. Nafion solution (5 wt%) was supplied by Sigma-Aldrich Chemical Reagent Co., Ltd. All chemicals were used without further purification.

Catalyst Synthesis

AuCuB-400 was prepared with following a slightly modified literature recipe.[1] $HAuCl_4 \cdot 3H_2O$ (40 μmol) and $CuCl_2 \cdot 2H_2O$ (40 μmol) were dissolved in DMF (4 mL), and the solution was sonicated until completely dissolved. Then $NaBH_4$ (400 μmol) was added with stirring at 0 °C using an ice bath. After stirred for 5 min, the material was centrifuged and washed with ethanol and water. Finally, the material was put into vacuum and dried at 60 °C for 8 h to obtain AuCuB-400. AuCuB-300 and AuCuB-500 were prepared by changing the amount of $NaBH_4$ to 300 μmol and 500 μmol. AuCu-400 catalyst was also synthesized in the same way excepted H_2O instead of DMF.

Material Characterizations

The morphology of the sample and lattice structure was characterized by a JEM-2100F Transmission electron microscope operated at 300 kV. The crystal structure of the sample was characterized by XRD [Ultima IV type with Cu-Kα as the X-ray source ($\lambda = 1.5406$ Å)]. X-ray photoelectron spectroscopy (XPS) adopted the AXIS Ultra DLD type to irradiate the material with an Al-Kα ray beam and used C 1s with a binding energy of 284.6 eV as the standard. The content of Cu, Au, and B in the sample is mainly determined by inductively coupled plasma-atomic emission spectrometry (ICP-AES) (Agilent 7700 Series).

The electrochemical CO_2 reduction

Preparation of the Working Electrode The working electrode was prepared by dropping the catalyst ink onto a carbon paper. This catalyst ink was prepared by dispersing 2 mg of as-synthesized catalyst in 20 μL of Nafion 117 solution and 40 μL of water, ultrasonicating for 30 min. The catalyst loading of all the catalysts on the carbon paper was 1 mg cm^{-2}.

CO_2 reduction and product analysis A gas diffusion electrode was used for CO_2 reduction. An anion exchange membrane was separated between the catholyte and anolyte chamber. A mass flow controller was used to set the CO_2 flow rate at 15 SCCM. A saturated calomel electrode (SCE) and Pt mesh electrode were utilized as the reference electrode and counter electrode, respectively. The electrocatalytic performance of two catalysts for the CO_2RR was conducted by LSV curves in an N_2-saturated (pH 14.0) or CO_2-saturated (pH 13.5) 1 M KOH electrolyte and a sweep rate of 50 mV s^{-1}. The measured potentials (V vs SCE) were converted to the RHE reference scale using $E_{RHE} = E_{SCE}+0.0591\times pH+0.241$ as previously reported.[2] Then, for product analysis, the GC (Agilent Technologies 7890A) with detected by thermal conductivity detector and flame ionization detector was used for the detection of gaseous and liquid products, Meanwhile, the liquid products were collected and analyzed using ^1H NMR technique. The Faradaic efficiency for a specific product is calculated using the following equation:

$$FE = Z\times n\times F/Q$$

The amount of substance represented by n; the number of electrons transferred by the product produced by Z; the value of F is 96485 F mol^{-1}; the total electrolytic electricity represented by Q. The partial current density for a specific product equals total current density multiplies Faradaic efficiency for this product.

Operando Raman Measurements

All in situ electrochemical experiments were performed in a custom-made three-electrode cell (Tianjin Aida Hengsheng Technology Development Co., Ltd.). Operando Raman spectra was taken on a Raman microscope (Renishaw) with a 633 nm excitation laser. The Raman probe was focused on the electrode/electrolyte interface through a quartz window. Raman spectra was collected during chronoamperometry at various potentials. All potentials which refered to Raman data discussed in the results were against the RHE and converted to the RHE scale by $E_{RHE} = E_{Ag/AgCl}+0.198+0.0591\times pH$.

Computational methods

The first-principles density functional theory (DFT) calculations with plane-wave basis set were performed using the Vienna ab initio simulation package (VASP) software.[3] All calculations used the generalized gradient approximation (GGA) with the projector-augmented wave (PAW)[4] pseudopotentials and the Perdew-Burke-Ernzerhof (PBE)[4] exchange-correlation functional. The plane wave cutoff energy was set to 400 eV. The convergence of energy and forces were 1×10^{-5} eV and 0.02 eV $Å^{-1}$ for structural optimization. The AuCu(111) and AuCu(111)-B surfaces were modeled by p(1×1) four-layer slabs and 15 Å of vacuum space was applied to eliminate the spurious interactions between slabs along the Z direction. The Brilouin zone was sampled with 7×7×1 Monkhorst-Pack mesh for structural relaxations and 14×14×1 for electronic structure analysis. The bottom layers were fixed while the top three layers were fully relaxed during structural optimization. The Gibbs free energy change (ΔG) for each CO_2RR process was given by

$$\Delta G = \Delta E + \Delta ZPE - \Delta TS$$

Where E can be directly obtained from DFT calculations, ZPE and TS were defined as zero-point energy and entropy change at room temperature (298.15 K), respectively.

Results and Discussion

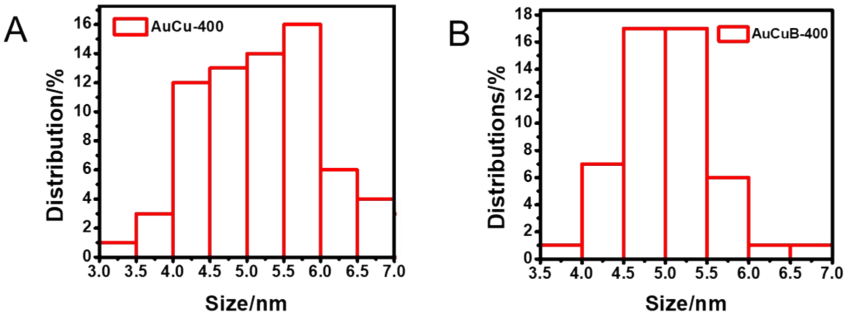

Figure S1. Histograms of the particle size distribution of AuCu-400 (A) and AuCuB-400 (B).

$$NaBH_4 \xrightarrow{DMF} Na^+ + BH_4^- \qquad (S1)$$

$$BH_4^- \xrightarrow{AuCu} \text{B-AuCu} \qquad (S2)$$

$$BH_4^- + H^+ \longrightarrow BH_5 \qquad (S3)$$

$$BH_5 \longrightarrow BH_3 + H_2 \qquad (S4)$$

$$BH_3 \xrightarrow{AuCu} \text{B-AuCu} + H_2 \qquad (S5)$$

Figure S2. The possible reactions for the formation of AuCuB

As $NaBH_4$ was added into DMF, Na^+ can be strongly solvated by DMF through coordination, allowing high dissolution of $NaBH_4$ and dissociation of borohydride anion (BH_4^-).[5] The BH_4^- anions can act as reductant for AuCu formation. Meanwhile, BH_4^- can also decompose on surface of AuCu to produce B atoms on the growing AuCu surface [Eq S1-S5].[6] As shown in Table S1, the decomposition of BH_4^- could also occurred on prepared AuCu or Cu (entries 4 and 6), unfortunately not on the surface of Au (entries 2 and 5).

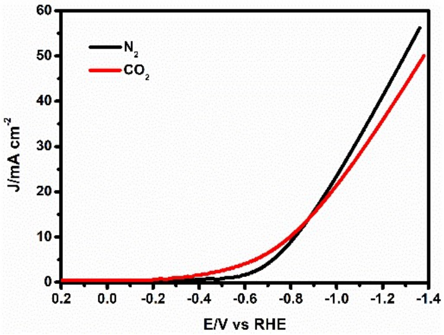

Figure S3. LSV curves recorded at a scan rate of 50 mV s^{-1} in 1 M KOH for AuCu-400.

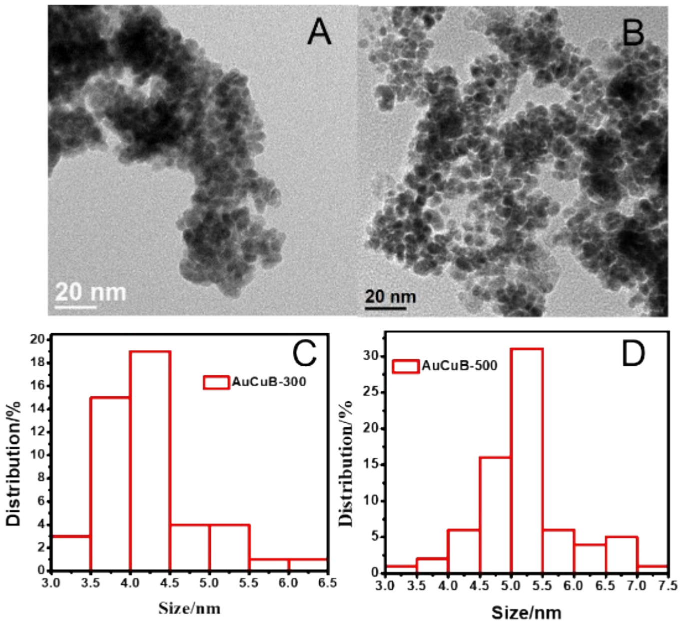

Figure S4. TEM images (A, B) and histograms of the particle size distributions (C, D) of AuCuB-300 (A, C) and AuCuB-500 (B, D).

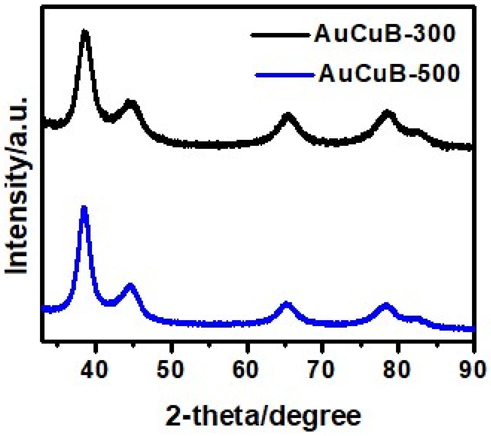

Figure S5. XRD patterns of AuCuB-300 (black line) and AuCuB-500 (blue line).

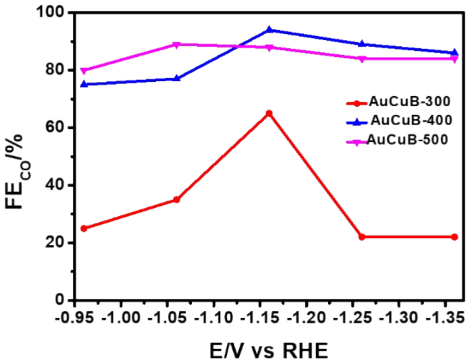

Figure S6. FE$_{CO}$ for different AuCuB electrocatalysts (AuCuB-300, AuCuB-400 and AuCuB-500).

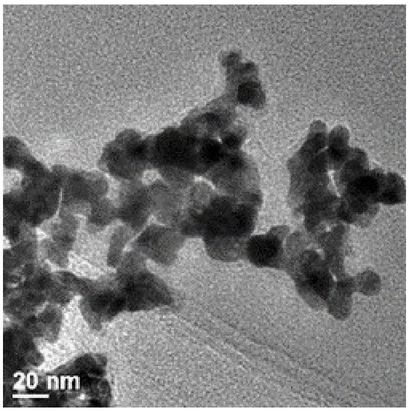

Figure S7. TEM image of the AuCuB-400 after electrolysis

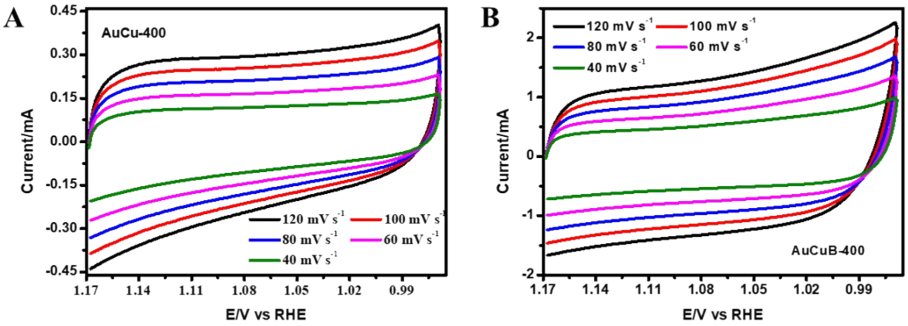

Figure S8. Cyclic voltammetry curves of AuCu-400 (A) and AuCuB-400 (B) at different scan rate (40 mV/s, 60 mV/s, 80 mV/s, 100 mV/s, and 120 mV/s).

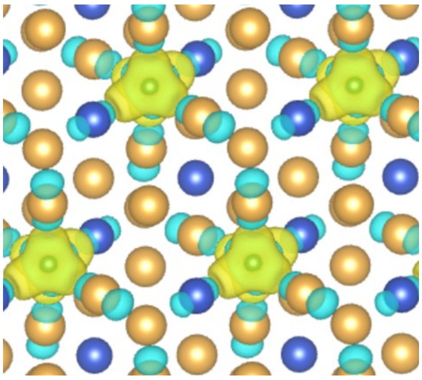

Figure S9. Charge density difference of the AuCuB model. The yellow and blue regions represent the electron accumulation and depletion, respectively. Au: large yellow, Cu: large blue, B: small green.

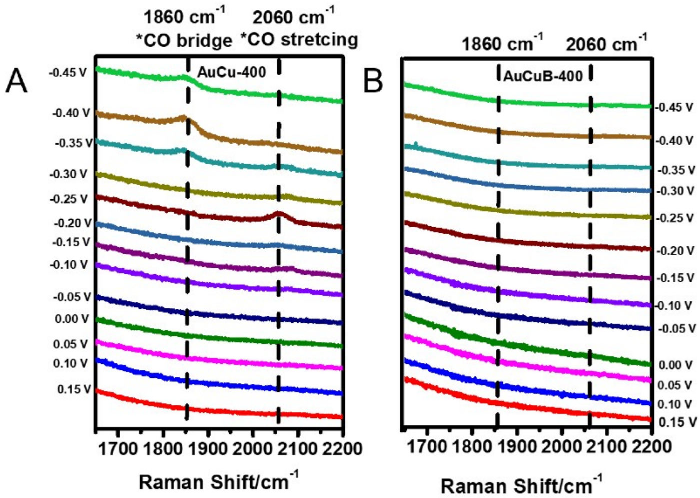

Figure S10. Potential-dependent Operando Raman spectroscopy recorded on AuCu-400 (A) and AuCuB-400 (B) in 1 M KOH.

According to the previous literature,[7] the mechanism was shown as follows, in general, it can be divided into following three steps [Eqs. (S6)-(S8)]：

$$CO_2 + * + H^+ + e^- \rightarrow *COOH \qquad (S6)$$

$$*COOH + H^+ + e^- \rightarrow *CO + H_2O(l) \qquad (S7)$$

$$*CO \rightarrow CO + * \qquad (S8)$$

* implies an adsorption site. CO_2 undergoes a proton-coupled electron transfer (PCET) step to give *COOH, which is further reduced to *CO after another PCET step. Finally, the adsorbed *CO is released from the surface as the product.

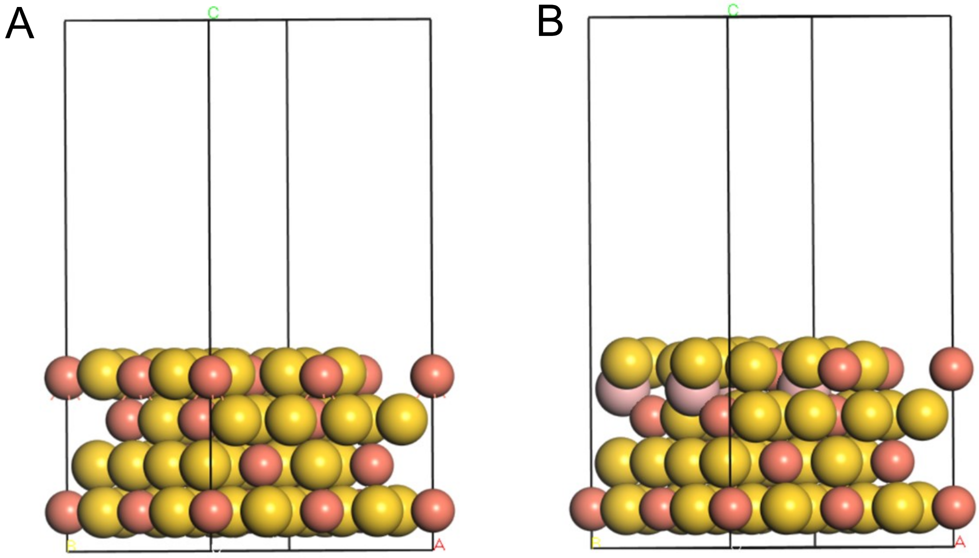

Figure S11. Computational models of the AuCu(111) (A) and AuCu(111)-B (B). Au: yellow, Cu: orange, B: pink.

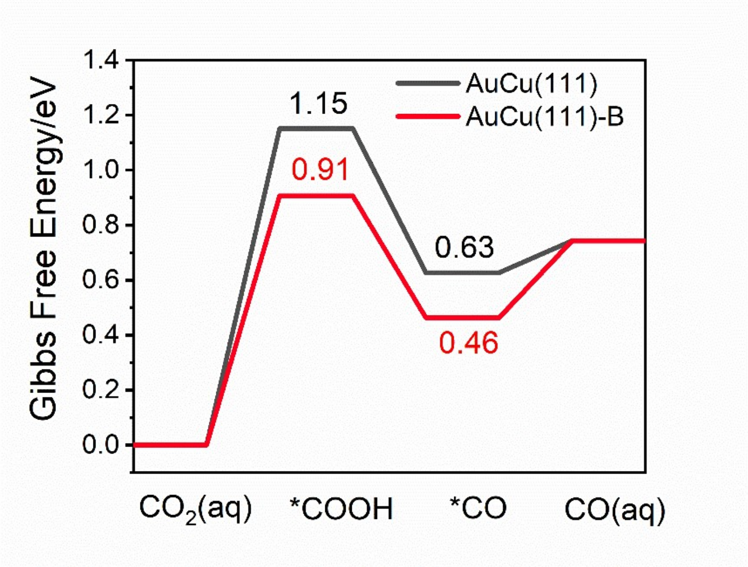

Figure S12. Gibbs free energy profiles of CO_2RR to CO on AuCu(111) and AuCu(111)-B calculated with VASPsol code, considering the solvation effect of water.

Table S1 Controlled experiments for the synthesis of AuCuB

Entry	Synthesis processes	Synthesized materials	B content (at%)
1	$HAuCl_4{\cdot}H_2O + CuCl_2{\cdot}2H_2O + NaBH_4 \xrightarrow[DMF]{}$	AuCuB	3.93
2	$HAuCl_4{\cdot}H_2O + NaBH_4 \xrightarrow[DMF]{}$	Au(B)	--
3	$CuCl_2{\cdot}2H_2O + NaBH_4 \xrightarrow[DMF]{}$	--	--
4	1) $HAuCl_4{\cdot}H_2O + CuCl_2{\cdot}2H_2O + NaBH_4 \xrightarrow[H_2O]{} AuCu$ 2) $AuCu + NaBH_4 \xrightarrow[DMF]{}$	AuCuB-2	1.2
5	1) $HAuCl_4{\cdot}H_2O + NaBH_4 \xrightarrow[H_2O]{} Au$ 2) $Au + NaBH_4 \xrightarrow[DMF]{}$	Au(B)-2	--
6	1) $CuCl_2{\cdot}2H_2O + NaBH_4 \xrightarrow[H_2O]{} Cu$ 2) $Cu + NaBH_4 \xrightarrow[DMF]{}$	CuB-2	0.7

Table S2 Summary of reported heteroatom-doped catalysts for CO production via CO_2RR.

Catalyst	Max FE_{CO} (%)	J_{CO} @MaxFE (mA cm^{-2})	Ref
AuCuB	99	76	this work
Ordered AuCu	75	78.3	[8]
MoSeS alloy monolayers	45.2	43	[9]
PdH(111) octahedra	92	40.2	[10]
Bi-CMEC	80	30	[11]
LiET-Zn	91.1	23	[12]
$Au_{94}Pd_6$	94	10	[13]
Ag/Pd alloys	98.6	9.3	[14]
$PdCu_3$/NC	99.2	4.45	[15]
NCNTs	80	0.75	[16]
N,S-Co doped carbon layers	92	2.63	[17]
F-C	90	0.26	[18]
3D-NG	85	1.8	[19]
g-C_3N_4/MWCNTs	60	0.6	[20]
ZIF-8 mediated NC	78	1.1	[21]
BNMC	95	3.0	[22]
NPCM	92	3.1	[23]

Table S3 B content (ICP-AES) with different $NaBH_4$ conditions

Kinds of Catalysts	B content (at%)
AuCuB-300	2.06
AuCuB-400	3.93
AuCuB-500	5.88

References

1. Z. Wang, J. Niu, Y. Xu, L. Wang, H. Wang and H. Liu, *ACS Sustainable Chem. Eng.*, 2020, **8**, 12588-12594.
2. W.-Y. Zhi, Y.-T. Liu, S.-L. Shan, C.-J. Jiang, H. Wang and J.-X. Lu, *Journal of CO2 Utilization*, 2021, **50**, 101594.
3. G. Kresse and J. Furthmüller, *Physical Review B*, 1996, **54**, 11169-11186.
4. P. E. Blöchl, *Physical Review B*, 1994, **50**, 17953-17979.
5. R. J. S. Francis A.Carey, *Advanced Organic Chemistry, Part A: Structure and Mechanisms, 5th Edition*, 2007.
6. J. Li, J. Chen, Q. Wang, W.-B. Cai and S. Chen, *Chem. Mater.*, 2017, **29**, 10060-10067.
7. X. Kong, Y. Liu, P. Li, J. Ke, Z. Liu, F. Ahmad, W. Yan, Z. Li, Z. Geng and J. Zeng, *Appl. Catal., B*, 2020, **268**, 118452.
8. Y. Han, Z. Wang, X. Han, W. Fang, Y. Zhou, K. Lei, B. You, H. S. Park and B. Y. Xia, *ACS Sustainable Chem. Eng.*, 2021, **9**, 2609-2615.
9. J. Xu, X. Li, W. Liu, Y. Sun, Z. Ju, T. Yao, C. Wang, H. Ju, J. Zhu, S. Wei and Y. Xie, *Angew. Chem. Int. Ed.*, 2017, **56**, 9121-9125.
10. W. Zhu, S. Kattel, F. Jiao and J. G. Chen, *Adv. Energy Mate*, 2019, **9**, 1802840.
11. J. Medina-Ramos, J. L. DiMeglio and J. Rosenthal, *J. Am. Chem. Soc.*, 2014, **136**, 8361-8367.
12. K. Jiang, H. Wang, W.-B. Cai and H. Wang, *ACS Nano*, 2017, **11**, 6451-6458.
13. S. Zhu, X. Qin, Q. Wang, T. Li, R. Tao, M. Gu and M. Shao, *J. Mater. Chem. A,*, 2019, **7**, 16954-16961.
14. D. L. T. Nguyen, T. M. Nguyen, S. Y. Lee, J. Kim, S. Y. Kim, Q. V. Le, R. S. Varma and Y. J. Hwang, *Environ. Res.*, 2022, **211**, 113116.
15. J. Dong, Y. Cheng, Y. Li, X. Peng, R. Zhang, H.-T. Wang, C. Wang, X. Li, P. Ou, C.-W. Pao, L. Han, W.-F. Pong, Z. Lin, J. Luo and H. L. Xin, *ACS Appl. Mater. Interfaces*, 2022, **14**, 41969-41977.
16. J. Wu, R. M. Yadav, M. Liu, P. P. Sharma, C. S. Tiwary, L. Ma, X. Zou, X.-D. Zhou, B. I. Yakobson, J. Lou and P. M. Ajayan, *ACS Nano*, 2015, **9**, 5364-5371.
17. F. Pan, B. Li, W. Deng, Z. Du, Y. Gang, G. Wang and Y. Li, *Appl. Catal., B*, 2019, **252**, 240-249.
18. J. Xie, X. Zhao, M. Wu, Q. Li, Y. Wang and J. Yao, *Angew. Chem. Int. Ed.*, 2018, **57**, 9640-9644.
19. J. Wu, M. Liu, P. P. Sharma, R. M. Yadav, L. Ma, Y. Yang, X. Zou, X.-D. Zhou, R. Vajtai, B. I. Yakobson, J. Lou and P. M. Ajayan, *Nano Lett.*, 2016, **16**, 466-470.
20. X. Lu, T. H. Tan, Y. H. Ng and R. Amal, *Chem.Eur.J*, 2016, **22**, 11991-11996.

21. R. Wang, X. Sun, S. Ould-Chikh, D. Osadchii, F. Bai, F. Kapteijn and J. Gascon, *ACS Appl. Mater. Interfaces*, 2018, **10**, 14751-14758.
22. X. Ma, J. Du, H. Sun, F. Ye, X. Wang, P. Xu, C. Hu, L. Zhang and D. Liu, *Appl. Catal., B*, 2021, **298**, 120543.
23. S. Chen, T. Liu, S. O. Olanrele, Z. Lian, C. Si, Z. Chen and B. Li, *Journal of Energy Chemistry*, 2021, **54**, 143-150.